Research Article

Dan Sui* and Juan Carlos Martinez Vidaur

Automated Characterization of Non-Newtonian Fluids Using Laboratory Setup

Abstract: The automation towards drilling fluid properties' measurement has been pursued in the recent years in order to increase drilling efficiency with less human intervention. Adequately monitoring and adjusting density and rheology of drilling fluids are fundamental responsibilities of mud engineers. In this study, experimental tests that automatically characterize fluids were conducted. The basic objective is to measure the differential pressures along two sections of the pipes: one horizontal section and one vertical section. Using such measuring data, mathematical algorithms are then proposed to estimate fluids' density and subsequently viscosity with respect to flow regimes, laminar and turbulence. The results were compared and validated with the values measured on rotational rheometers. With the help of models and numerical schemes, the work presented in the paper reveals a good opportunity to improve the accuracy and precision of continuous-measuring and monitoring fluids' properties.

Keywords: Automation, density and viscosity, Non-Newtonian fluids, experimental work

1 Introduction

Drilling fluids fulfil different functions during drilling and well construction processes. Two of the most important ones are: providing the energy required to control wellbore pressures, and carrying drilling cuttings out of wells. These two crucial functions' performances are mainly dependent on two of fundamental fluids' properties, density and viscosity. The most widely techniques used to measure them are mud balances and rotational rheometers respectively. However, they both are subject to measurement errors and assessments done by a person who takes mud samples and operates the equipment. Such role has typically been assigned to mud engineers and derrick man in a drilling rig to take measurement manually. The accuracy of fluids' properties measurements has been increased over time with the introduction of pressurized mud balances and digital rheometers. Many research works have been published to improve the measurement accuracy using rheometers. For instance, Dakhil and Wierschem [1] modified a commercial rheometer so that samples can be studied at gap widths well below the absolute error of commercial rheometers. Duffy et al. [2] proposed a novel empirical method for determining strain/strain rate and stress constants for non-standard measuring systems on rotational rheometers. Marchesini et al. [3] performed an experimental and numerical investigation of different rheometric flows of yield stress materials to analyse the flow pattern and apparent wall slip in rheological measurements of yield-stress materials in rotational rheometers.

During real time operations, rheometer measurements are only available when an operator runs a check, which at best occurs every roughly 15mins for density measurement and a few times per day for rheology measurement. Although one has to agree that routine viscosity check shall be done along with density measurement, the results of this quick analysis are most likely for reference purposes and provide little insight of the full rheological profile of fluids. Furthermore, when these tests are run, since only a limited volume of samples are collected from active mud pits for viscosity and density check, the assumption that it is representative of the considerably large volume of fluids pumped into the well may lead to gross errors.

In practice, we have limited information of fluids' properties in boreholes. As drilling wells becomes more challenging, there is an increased demand for having good knowledge and models to describe drilling fluids' behaviours. In the light of such demand, many research activities including modelling and experimental work have been performed. Takeh and Shanbhag [4] proposed and implemented a computer program in an open-source platform to infer the continuous and discrete relaxation spec-

*Corresponding Author: Dan Sui: Energy and Petroleum Engineering Department, University of Stavanger, Stavanger, Norway; Email: dan.sui@uis.no
Juan Carlos Martinez Vidaur: Energy and Petroleum Engineering Department, University of Stavanger, Stavanger, Norway

tra from small amplitude oscillatory shear experiments. Borg and Paakkonen [5] derived viscoelastic constitutive equations from control theory and developed formulas for the relaxation modulus, shear viscosity and dynamic viscosity. Saasen and Hodne [6] described how drilling fluids' viscous properties alter when being exposed to vibrations. Hernandez *et al.* [7] showed that wall slip leads to the underestimation of the magnetic field-induced yield stress when measuring geometries with smooth surfaces. Carmona *et al.* [8] explored the rheology of an advanced performance xanthan gum, which is able to endure the shear and turbulent flows. Saasen and Ytrehus [9] presented a viscosity model of the Herschel-Bulkley type where the shear rate is made dimensionless by selecting a characteristic shear rate for the flow. Skadsem and Saasen [10] focused on typical oil field viscometers and discussed effects of yield stress and shear thinning on fluid yielding at low viscometer rotational speeds and errors caused by the Newtonian shear rate assumption.

Moreover, the demand towards automated charactering and controlling fluids' properties in a more systematic and consistent way becomes increasing. This is where drilling automation comes into play. A more thorough monitoring and control of drilling fluids' properties reduces risks of drilling problems associated with inadequate wellbore pressures, which ultimately becomes safer and less expensive drilling operations. Such concept has been proposed recently. For example, Saasen *et al.* [11] demonstrated a yard trial for automatic measurement of drilling fluids' properties, like particle size distribution, concentration and morphology, viscosity and produced cuttings volume. Vajargah *et al.* [12] presented experimental tests for automated calculations of drilling fluids' properties with the use of a pipe viscometer. Skadsem *et al.* [13] reported a detailed rheological characterization of a water-based drilling fluid and an invert emulsion oil-based drilling fluid and analysed the shear rate step change measurements using a structural kinetics thixotropy model. In terms of successful industrial examples, Stock *et al.* [14] provided a good overview and introduction of industrial control systems and devices used for drilling fluids' propterty measurements and monitoring. For instance, coriolis fluid density unit and automated rheometer have been used for continuous density and viscosity measurements.

From 2013, we have been working on fluids' properties automatic evaluation and published many related works, see [15–17]. The aim of our work is to have good proof of concept tests for automated fluids' properties measurements in a laboratory scale system, that could potentially be the basis for a real-time monitoring arrangement. In our study, different friction factor models have been compared in terms of the viscosity calculations in order to improve the accuracy and precision of proposed approach. The data acquisition system and proposed numerical algorithms show a high accuracy of the viscosity and density calculations of non-Newtonian solids-free fluids in different flow regimes. Such automated measurement is a promising concept for downhole fluids properties' monitoring and control.

2 Experimental setup

The idea behind this proposed standpipe concept is to use differential pressure sensors installed in surface connections of the circulating system in a drilling rig, in order to measure differential pressures continuously that would then be used to calculate density and viscosity of fluids being pumped into the well. Such concept has been proposed and demonstrated in [15, 16]. Based on such idea, one experimental system was setup at University of Stavanger, Norway in 2016 for testing and evaluation. Figure 1 illustrates a simplified schematic of this instrumented standpipe concept. In the experimental system, there are two differential pressure sensors installed, one in a horizontal section, and one in a vertical section. In the schematic, the horizontal differential pressure between pressure sensors 1 and 2 is given by dP_{hor} ; whereas the vertical differential pressure between pressure sensors 3 and 4 is denoted as dP_{ver}.

The working principle is to measure the pressure, dP_{hor}, and since there is no gravitational effect on the horizontal section of the pipe, all pressure losses in this segment are presumed to be caused by viscous friction. The differential pressure in the vertical section, dP_{ver}, is the result of both frictional pressure losses and hydrostatic pressure. In this experimental setup, the size, the length, and the roughness of the pipe are assumed to be the same in both sections. Thus the frictional pressure losses are equal in both pipe segments. Consequently, the difference between dP_{ver} and dP_{hor} is equivalent to the hydrostatic pressure, which is then used to back calculate the fluid density. Once the fluid density is determined, the fluid viscosity can be calculated from the friction models. In the following sections, we will introduce detailed calculation steps.
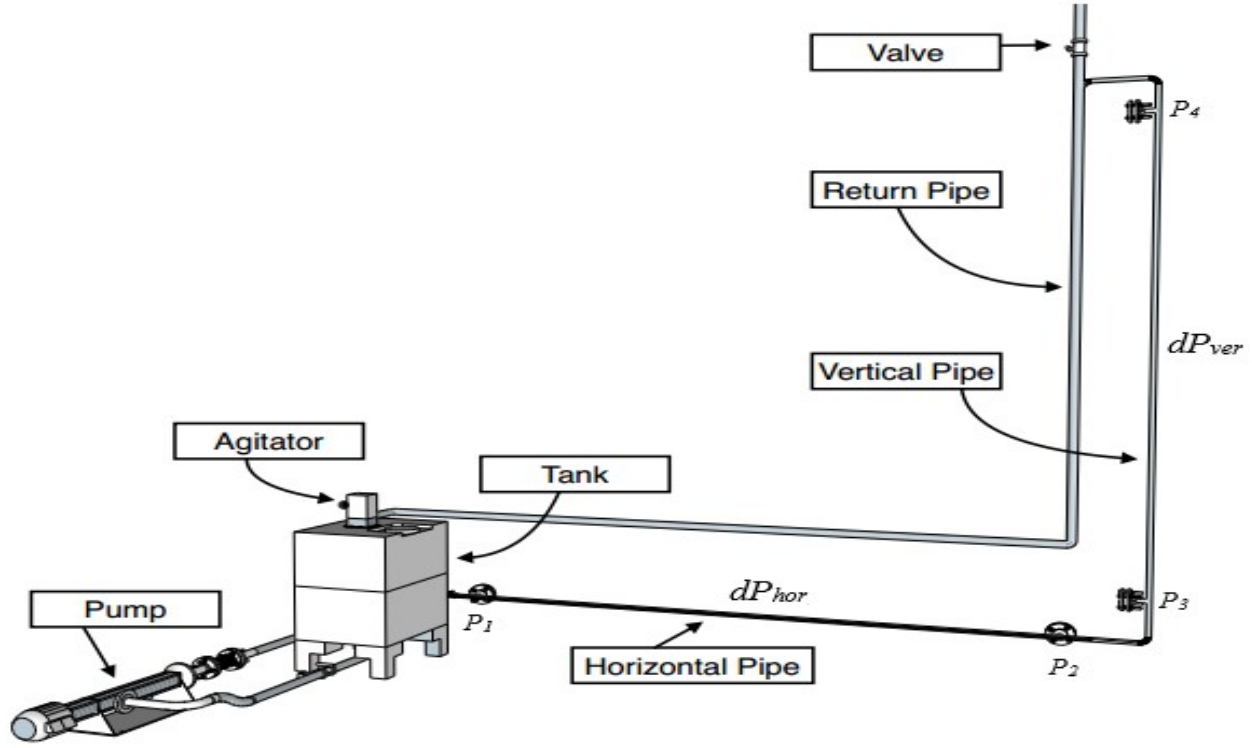
Figure 1: Simplified schematic of the instrumented standpipe concept.

3 Density calculations

Given that the pipe characteristics, flow properties, and distance between sensors are the same in both the vertical and the horizontal sections, we state the following correlation:

$$\Delta P_{\text{Hydrostatic}} = dP_{\text{ver}} - dP_{\text{hor}}. \tag{1}$$

The hydrostatic pressure between two pressure sensors P_3 and P_4 is

$$\Delta P_{\text{Hydrostatic}} = \rho g \Delta h, \tag{2}$$

where ρ is the fluid density, g is the acceleration of gravity and Δh is the vertical distance between sensors P_3 and P_4. Combining Equations (1) and (2), we obtain

$$\rho = \frac{dP_{\text{ver}} - dP_{\text{hor}}}{g \Delta h}. \tag{3}$$

The parameters involved in Equation (3) are known, *i.e.* dP_{ver} and dP_{hor} are measured through the differential pressure sensors. Thus the fluid property, density (ρ), can be determined by Equation (3).

4 Friction factor calculation

The concept of frictional pressure losses derives from the resistance experienced by fluids flowing through pipes caused by the friction against pipe walls. The frictional pressure loss is determined from the Darcy-Weisbach equation given below:

$$\Delta P_{\text{Frictional}} = \frac{fL\rho v^2}{2D}, \tag{4}$$

where f is the friction factor, L is the pipe length, v is the average fluid velocity and D is the pipe inner diameter. The average fluid velocity can be calculated by the pump rate and cross-sectional area of pipe:

$$v = Q/A, \tag{5}$$

where Q is the pump rate and A is the pipe cross-sectional inner area. In our experimental study, it is assumed that the horizontal differential pressure is caused solely by frictional pressure losses. Therefore, we have

$$dP_{\text{hor}} = \Delta P_{\text{Frictional}}. \tag{6}$$

Then, Equation (4) is rearranged to obtain the following correlation:

$$f = \frac{2D dP_{\text{hor}}}{L\rho v^2}. \tag{7}$$

Now, from the basic definition given in Equation (5), and in terms of the known parameters (D, L, ρ, Q), the friction factor can be determined through:

$$f = \frac{\pi^2 D^5 \mathrm{dP_{hor}}}{8L\rho v^2}. \tag{8}$$

All parameters in Equation (8) are given or directly measured, thus, the friction factor can then be calculated and subsequently used to determine the adequate Reynolds number and flow regime.

5 Viscosity calculations

5.1 Laminar flow

We start the calculations for the laminar flow. In the following equation, τ_w is the shear stress at the wall. Following [18–21], it is easy to get the correlation between pressure losses and the shear stress:

$$\tau_w 4L = \Delta P_{\mathrm{Frictional}} D. \tag{9}$$

Once the horizontal pressure losses $\mathrm{dP_{hor}}$ is obtained from the experimental runs, the shear stress can be calculated with Equation (9) which is reformulated as follows,

$$\tau_w = \frac{D\mathrm{dP_{hor}}}{4L}. \tag{10}$$

From the derivations given in Appendix A1, we have

$$\gamma_w = \frac{8v}{D} \frac{3n_a + 1}{4n_a}, \tag{11}$$

where γ_w is the shear rate at the wall, n_a is the generalized flow index defined as

$$n_a = \frac{\partial \ln \tau_w}{\partial \ln \left(\frac{8v}{D}\right)}. \tag{12}$$

Once the shear stress and shear rate are obtained, the viscosity can be calculated as

$$\mu_a = \frac{\tau_w}{\gamma_w}. \tag{13}$$

For the above equations, only unknown parameter is the general flow index n_a. From its definition given in (12), it is difficult to find an analytical mathematical expression of n_a. Therefore we propose a numerical scheme (Algorithm 1) to estimate n_a by operating a series of experiment runs with decreasing flow rates. For each horizontal differential pressure value, we introduce two additional parameters, a and b:

$$a(i) = \ln \tau_w(i) \tag{14}$$

and

$$b(i) = \ln \frac{8v(i)}{D} \tag{15}$$

where i refers to i-th experimental run. Thus, we can approximate n_a by the following expression:

$$n_a(i) = \frac{a(i) - a(i-1)}{b(i) - b(i-1)}. \tag{16}$$

In summary, the numerical algorithm running to calculate the viscosity in laminar flow with different flow rate $Q(i)$ is presented below:

Algorithm 1 (Laminar flow)

Step 1: set $i = 1$,

Step 2: set the pump rate at $Q(i)$, where $Q(1)$ is set as maximum,

Step 3: measure the horizontal pressure loss $\mathrm{dP_{hor}}(i)$ with such flow rate $Q(i)$,

Step 4: calculate $\tau_w(i)$ from Equation (10),

Step 5: calculate $a(i)$ and $b(i)$,

Step 6: calculate $n_a(i)$ from Equation (16) when $i > 1$,

Step 7: calculate $\gamma_w(i)$ from Equation (11) when $i > 1$,

Step 8: calculate the viscosity from Equation (13) when $i > 1$,

Step 9: set $i = i + 1$, and decrease the flow rate by $Q(i) = Q(i-1) - \Delta Q$, where ΔQ is the defined increment for adjusting the flow rate,

Step 10: go to Step 2 until $Q(i)$ is less than some predetermined threshold,

Step 11: stop the experimental runs.

Above methodology is valid solely for laminar flow. The details of the analysis for transition and turbulent flow are described in the next subsection.

5.2 Turbulent flow

Given that Equation (11) was developed exclusively for fully developed laminar flow, it is no longer applicable to model the fluid characteristics in the turbulent region. From Appendix A2, the viscosity can be calculated for Herschel-Bulkley models as

$$\mu_a = \tau_0 \left(\frac{3n_a + 1}{4n_a} \frac{8v}{D}\right)^{-1} + K\left(\frac{3n_a + 1}{4n_a} \frac{8v}{D}\right)^{n-1} \tag{17}$$

where τ_0 is the yield point, K is the consistency index and n is the flow index. To obtain μ_a, it is necessary to determine the generalized flow index n_a. However, to the best knowledge of authors, there is no good approach to calculate n_a for turbulent flow. The solution proposed here is to

use a numerical shooting method [22] to find an adequate friction factor that models more accurately the horizontal pressure losses recorded with the experimental setup.

To specify it, we start to define two initial guesses of n_{a1} and n_{a2}, then based on such values, we calculate two viscosities μ_{a1}, and μ_{a2}, accordingly following Equation (17). The corresponding pressure losses ΔP_1 and ΔP_2 can be easily calculated, see the calculation procedure in Appendix A2. Such calculated values ΔP_1 and ΔP_2 then are compared with the measurement dP_{hor}. If the differences between ΔP_1, dP_{hor} or ΔP_2, dP_{hor} are greater than a specified tolerance (as a terminal condition), we adjust initial guesses n_{a1} and n_{a2}, and the process is repeated until the difference between them is less than such threshold.

The shooting method for determining the generalized flow index n_a, in turn, μ_a, based on the measured pressure loss is summarized below:

Algorithm 2 (Shooting method for calculating μ_a)

Step 1: set the pump rate at Q and measure the horizontal pressure loss dP_{hor},

Step 2: select two initial guesses for the generalized flow index n_{a1} and n_{a2} ($n_{a1} < n_{a2}$),

Step 3: calculate the viscosity μ_{a1} and μ_{a2} from n_{a1} and n_{a2} respectively using Equation (17),

Step 4: calculate the pressure loss ΔP_1 and ΔP_2 from μ_{a1} and μ_{a2} respectively using Equation (A17) (in Appendix A2) and one selected friction factor model listed in Table A1 (in Appendix A2),

Step 5: check the sign of e_1 and e_2, where

$$e_1 = \Delta P_1 - dP_{hor}, \quad e_2 = \Delta P_2 - dP_{hor},$$

Step 6: if $e_1 e_2 > 0$, choose new initial guesses of n_{a1} and n_{a2}, and go to Step 3; else go to Step 7,

Step 7: cut the interval $[n_{a1}, n_{a2}]$ into two halves and set $n_{a3} = (n_{a1} + n_{a2})/2$,

Step 8: calculate the viscosity μ_{a3} and the corresponding ΔP_3, and set $e_3 = \Delta P_3 - dP_{hor}$,

Step 9: if $e_3 < \eta$ (η is the defined tolerance), go to Step 11,

Step 10: if $e_1 e_3 < 0$, set $n_{a2} = n_{a3}$, else set $n_{a1} = n_{a3}$, go to Step 7,

Step 11: set $\mu_a = \mu_{a3}$.

The solution was to include a weight function in the MATLAB scripts, and by trial and error, find the most adequate combination of values that would yield the best approximation of the fluid viscosity. In Algorithm 2, if the error(e_3) is greater than a certain tolerance value(η), the

process is restarted from Step 7. The iteration is repeating the calculations until the tolerance value is met. For such numerical scheme, the selection of the initial guesses (n_{a1} and n_{a2}) is ad hoc. From Equation (A14), the range n_a is between 0 and 1. Thereby, one way to select the initial guesses is to let n_{a1} be close to 0 and n_{a2} be close to 1 in order to meet the condition ($e_1 e_2 < 0$). Once the generalized flow index n_a is determined, the viscosity is easily calculated by Equation (17) from Step 11. For friction factor calculations, there are different friction factor models listed in Table A1. In our study, we also take advantage of our approach to evaluate different friction models by comparing with the calculated viscosities and the ones measured by rotational viscometer. More discussions will be provided in Section 6.

6 Experimental study

The formulation presented in Table 1 includes two additional additives, MAGOX and NULLFOAM to improve the performance of the slurry, namely, a pH buffer and a defoamer. MAGOX is added to effectively buffer alkalinity to a maximum pH of 10.0 in order to allow the Xantham Gum Polymer (XCD) to fully yield, and NULLFOAM is added to prevent foaming in water-based drilling fluids. All materials were supplied by Schlumberger M-I SWACO.

In order to verify the applicability of the mathematical models for different fluids' viscosities, five different formulations were selected to be tested. The only variable component is the concentration of viscosifier (XCD), thus the higher the XCD concentration, the more viscous the fluid is. The concentrations were obtained from the recommended values endorsed by the supplier (Schlumberger M-I SWACO). The following table encompasses the fluid formulations analysed in this work.

Table 1: Fluid formulations

Additive	F1	F2	F3	F4	F5
MAGOX(10^{-3}mg/l)	0.25	0.25	0.25	0.25	0.25
XCD(g/l)	2	3	4	5	6
NULLFOAM(%vol)	0.5	0.5	0.5	0.5	0.5

6.1 Density calculation

The density of each of the formulations was measured using a previously calibrated pressurized mud balance. The recorded values were close to $1000 kg/m^3$ at room temperature (approximately 15 degree). We have arbitrarily set an acceptable tolerance of ±0.015 SG for the density results, which is portrayed by the black curves in Figure 2.

The estimated density of Formulation 1 using the flowloop setup, as illustrated in Figure 2, has a maximum error of 0.006 SG, which is within an acceptable tolerance for the purpose of this investigation. The estimated density of other formulations shows the similar results as the one shown in Figure 2.

6.2 Viscosity calculation

6.2.1 From viscometer data

For validations and comparisons, the rheological readings for each fluid formulation obtained with the Fann Model 35 Viscometer are listed in Table 2. It is important to point out that the readings presented below were collected at room temperature (approximately 15 degree), and they were verified by double-checking one sample with multiple viscometers. The samples of each formulation were collected from the flowloop tank after circulating the system for 20 minutes; the stability of the rheology was verified after 72 hours in the tank. The viscometer readings are shown in Figure 3.
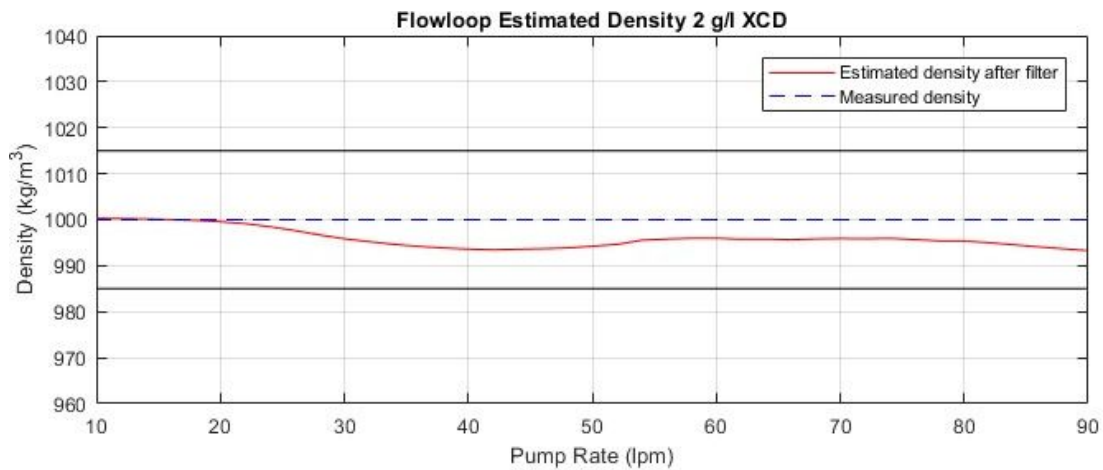

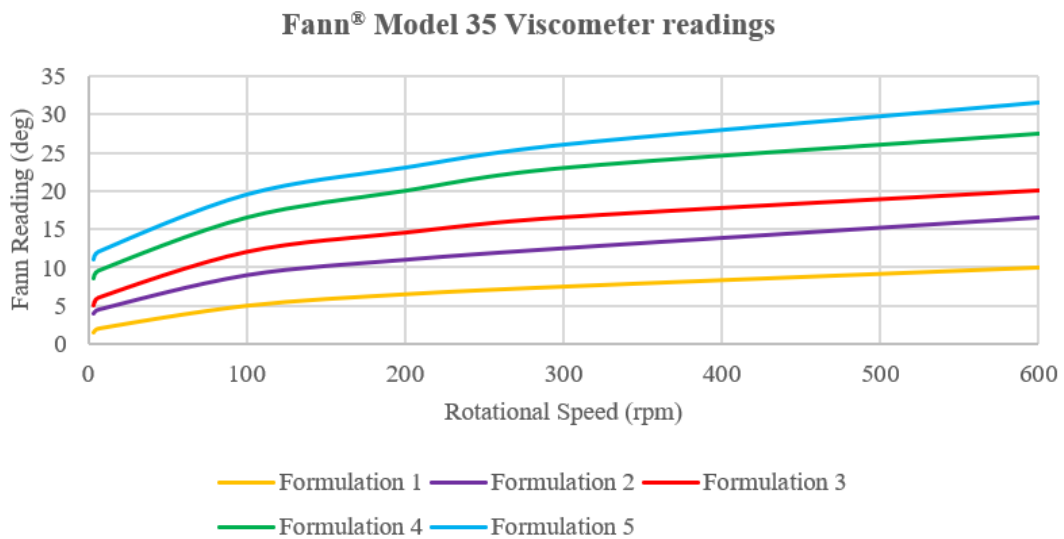**Figure 2:** Estimated density of Formulation 1

Figure 3: Comparison of Fann Model 35 Viscometer readings

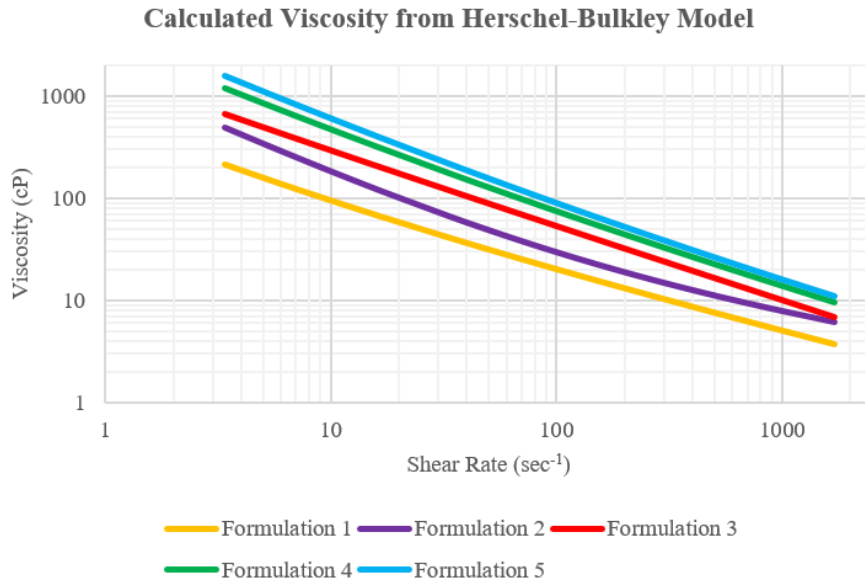**Calculated Viscosity from Herschel-Bulkley Model**

Figure 4: Composite of calculated viscosity using the Herschel-Bulkley model

The formulations perform Herschel-Bulkley rheological fluids. Using the Herschel-Bulkley models for each formulation, it is easy to calculate the viscosities with respect to different shear rates. Figure 4 shows the data in a log-log scale where the dimensions are shear rate (s^{-1}) and viscosity (cP). The plots were generated for each of the five formulations based on the data set presented in Table 2.

Table 2: Viscometer readings of each of the fluid formulations

Speed	F1	F2	F3	F4	F5
600	10	16.5	20	27.5	31.5
300	7.5	12.5	16.5	23	26
200	6.5	11	14.5	20	23
100	5	9	12	16.5	19.5
6	2	4.5	6	9.5	12
3	1.5	4	5	8.5	11

6.2.2 From flowloop data

As what we have discussed in Section 5, there are lots of friction factor models existed for friction factor calculations. Since most of models are empirical based on experimental data, there is no standard criteria to evaluate and verify them. In order to have an accurate viscosity calculation, we compared the viscosity calculations with different

friction factor models listed in Table A1. Figure 5 shows the comparisons using the flowloop data of Formulation 5.

In Figure 5, the blue curve depicts the Herschel-Bulkley fluid viscosities obtained from the Fann Model 35 Viscometer readings as a reference line, the other curves show the viscosities calculated from Algorithm 1 and Algorithm 2 with respect to different flow regimes using different friction factor models listed in Table A1. For the laminar flow, the viscosity is unique with respect to the flow rate. However, for the turbulence flow, the calculated viscosity varies seriously due to the choice of different friction factor models. From Figure 5, it is easy to see that the model by Thomas (see Table A1) provides the best approximation. Such observation is also obtained from other 4 formulations. Therefore, the plots to be presented below were generated based on the calculations using Thomas's model.

From Figure 6 to Figure 10, the blue curve depicts the fluid viscosities obtained from the Viscometer readings (marked as Modeled Viscosity HB); the red points are the viscosity values calculated using Algorithm 1 with ignoring the flow regime (always assume it is the laminar flow), marked as Flowloop Rabinowitsch; and the purple markers represent the fluid viscosities generated with the Thomas's correlation using Algorithm 2, marked as Flowloop Thomas. From Figures 6-10, we can draw some conclusions regarding the accuracy of the fluid viscosity estimations. It is observed that the calculated viscosities match the Herschel-Bulkley values until certain point at which the mismatch becomes evident. We decided to investigate the effect of the flow regime in this behaviour;
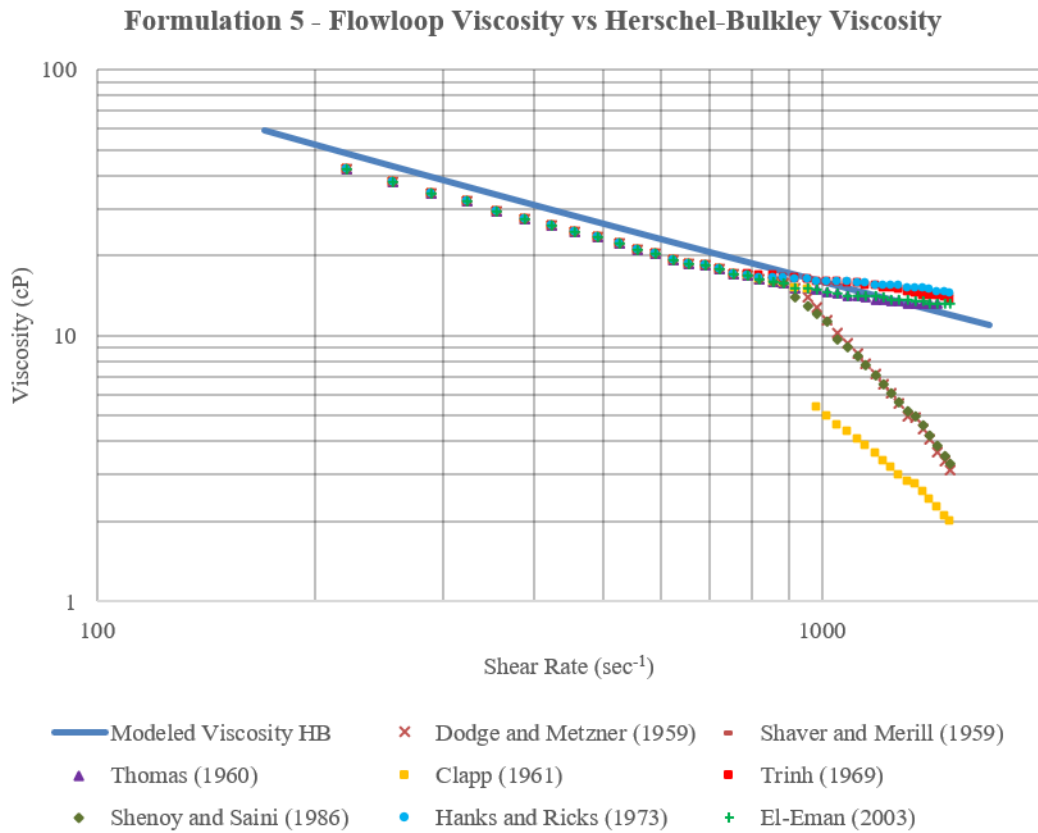
Figure 5: Estimated viscosity of Formulation 5 from flowloop data using different friction factor models given in Table A1
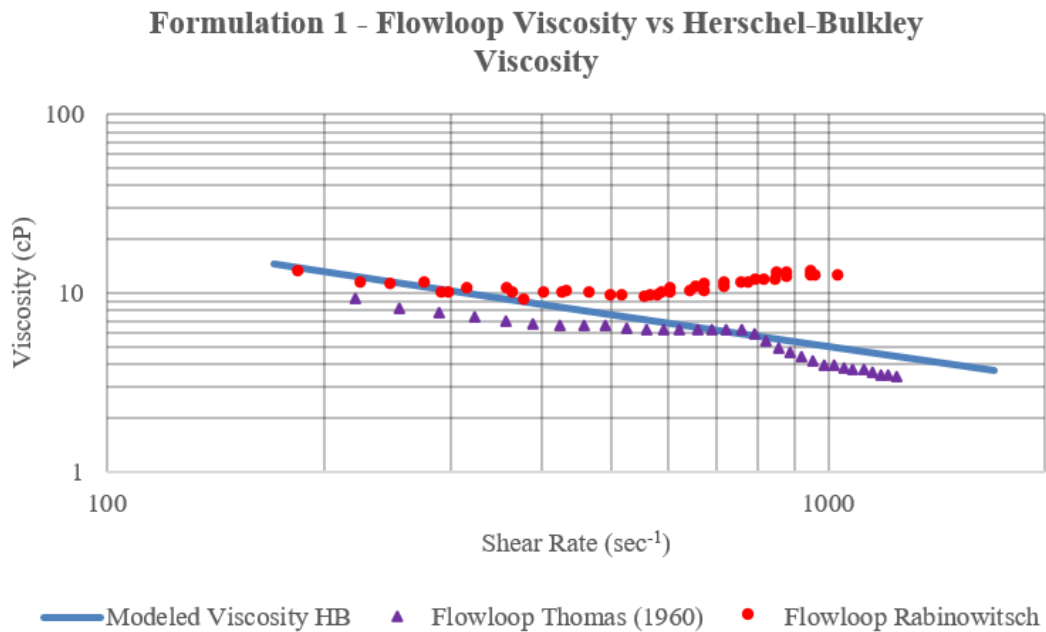

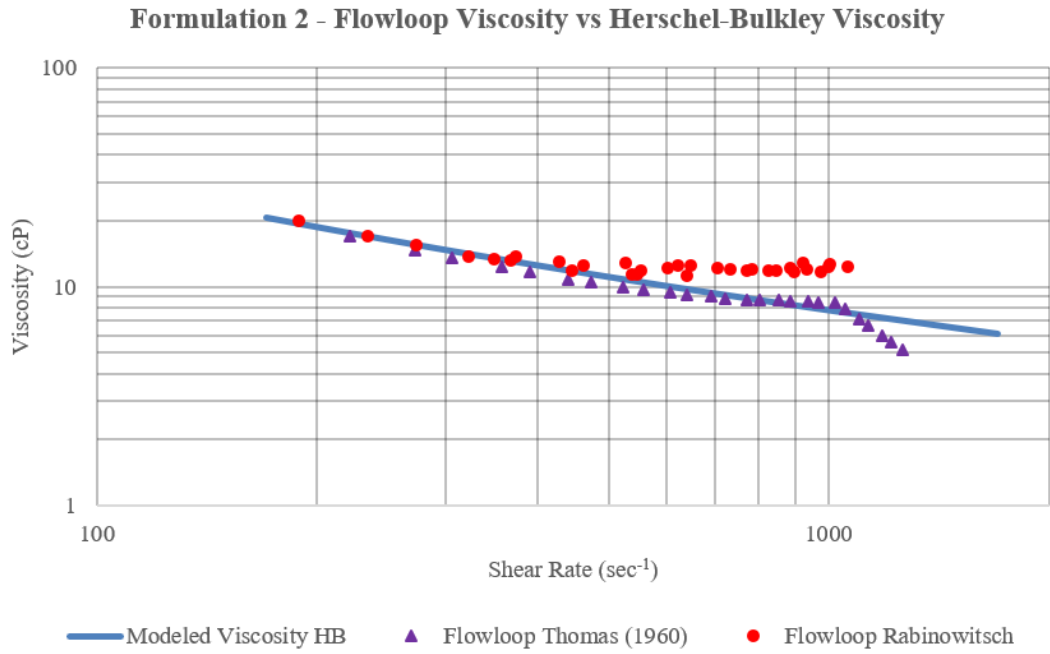**Figure 6:** Estimated viscosity of Formulation 1
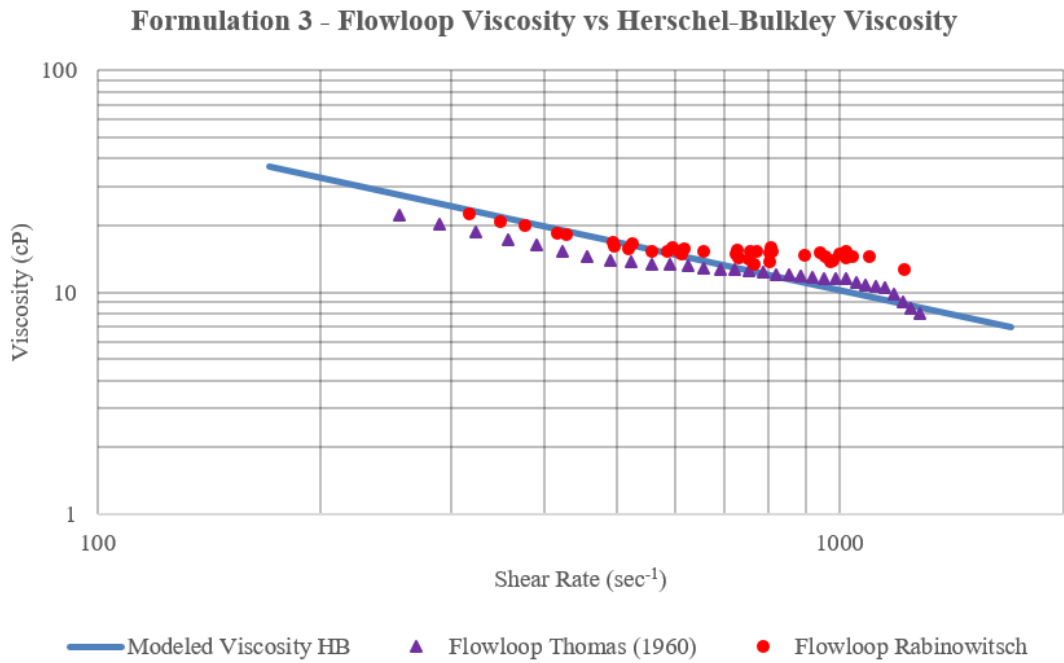
Figure 7: Estimated viscosity of Formulation 2

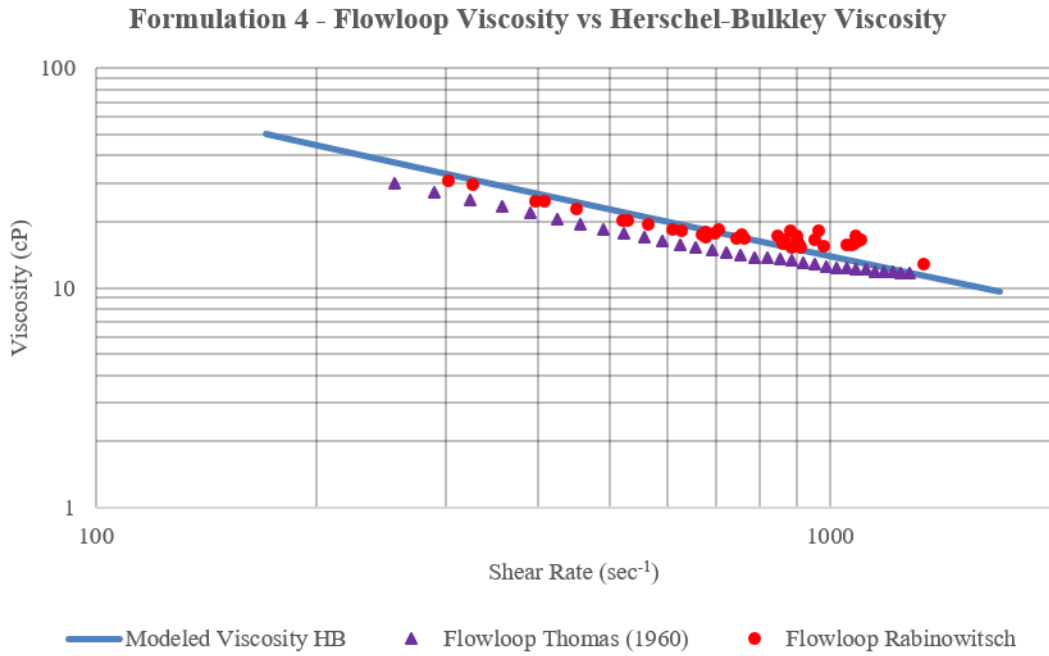**Figure 8:** Estimated viscosity of Formulation 3

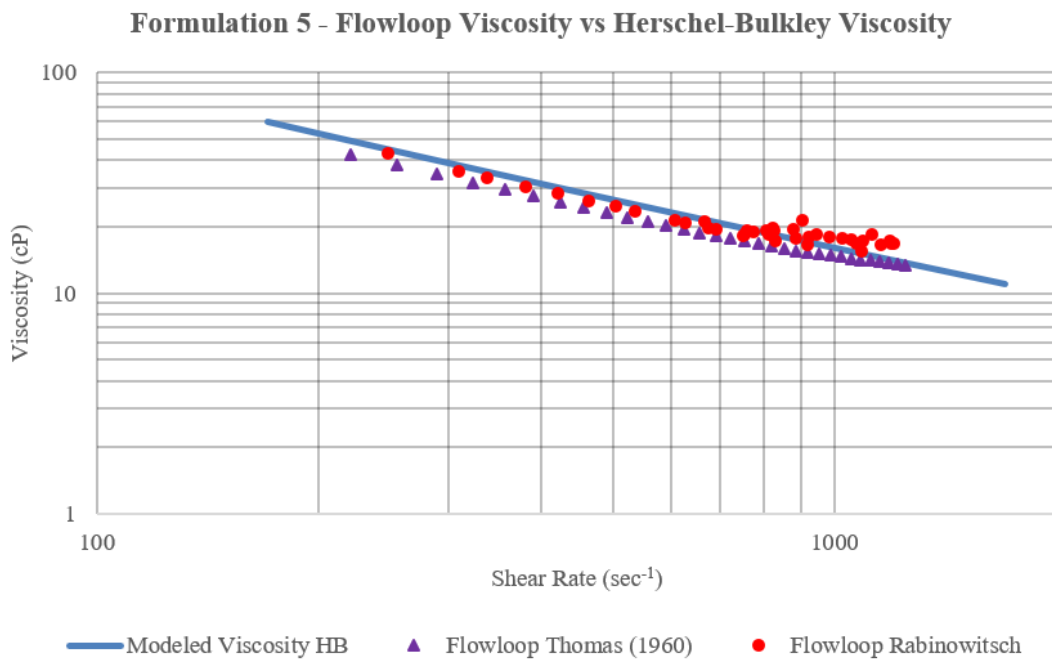**Figure 9:** Estimated viscosity of Formulation 4

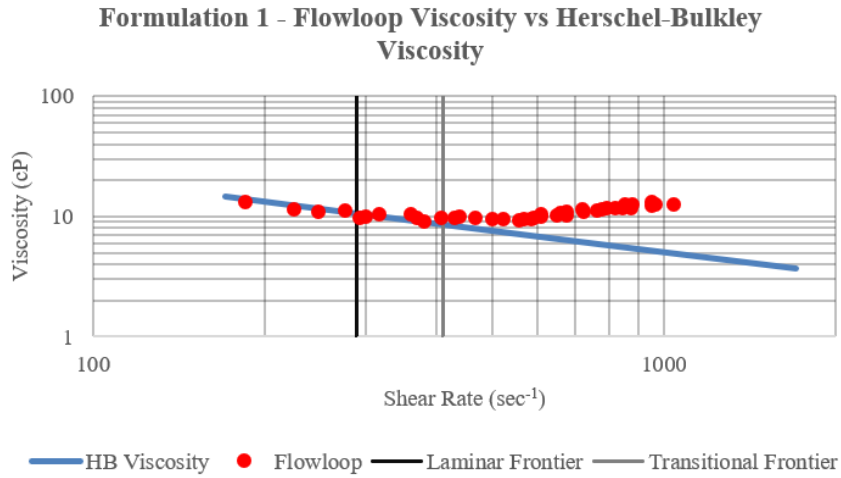**Figure 10:** Estimated viscosity of Formulation 5

Figure 11: Formulation 1 - Flowloop Viscosity vs Herschel-Bulkley Viscosity
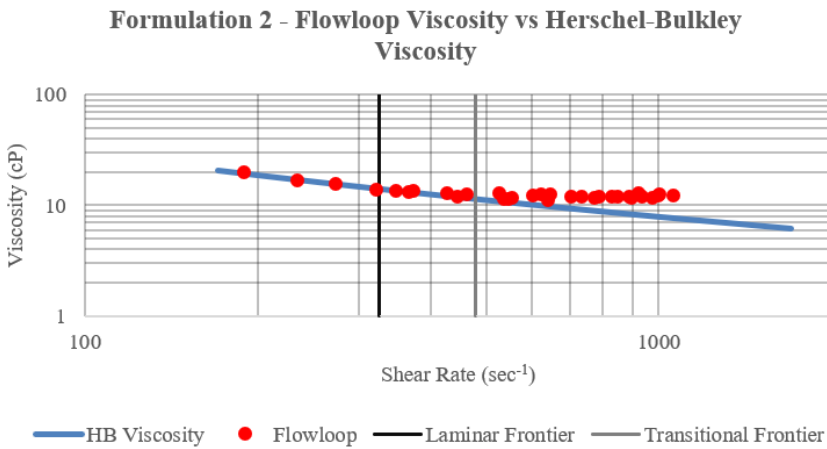

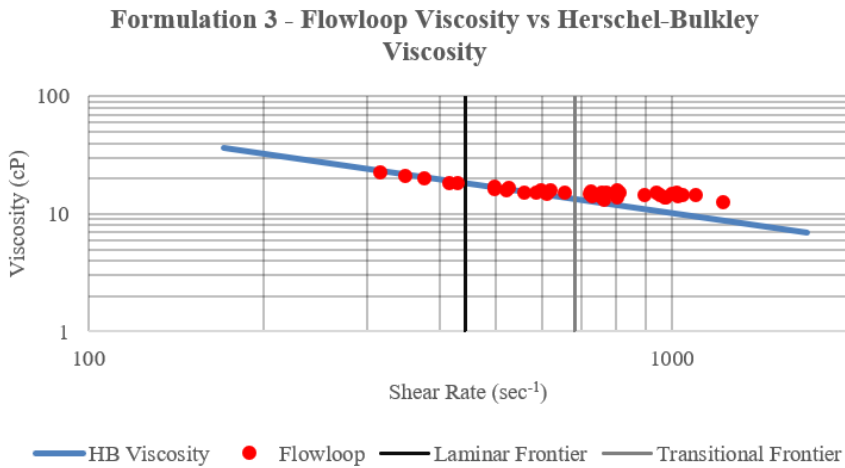**Figure 12:** Formulation 2 - Flowloop Viscosity vs Herschel-Bulkley Viscosity

Figure 13: Formulation 3 - Flowloop Viscosity vs Herschel-Bulkley Viscosity
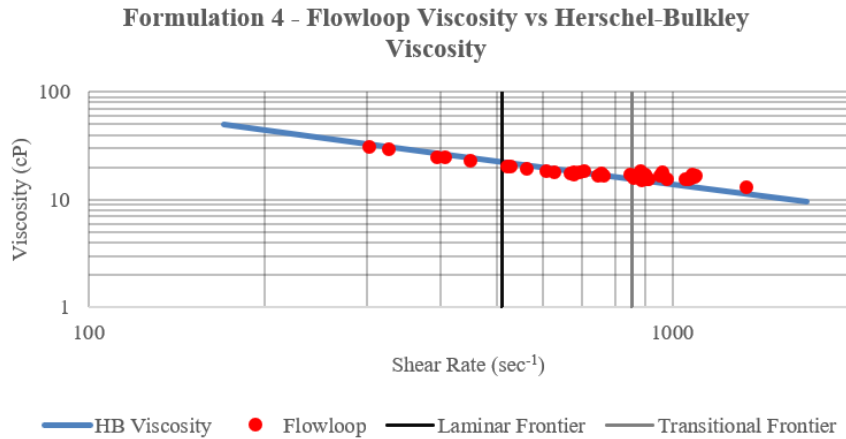
Figure 14: Formulation 4 - Flowloop Viscosity vs Herschel-Bulkley Viscosity
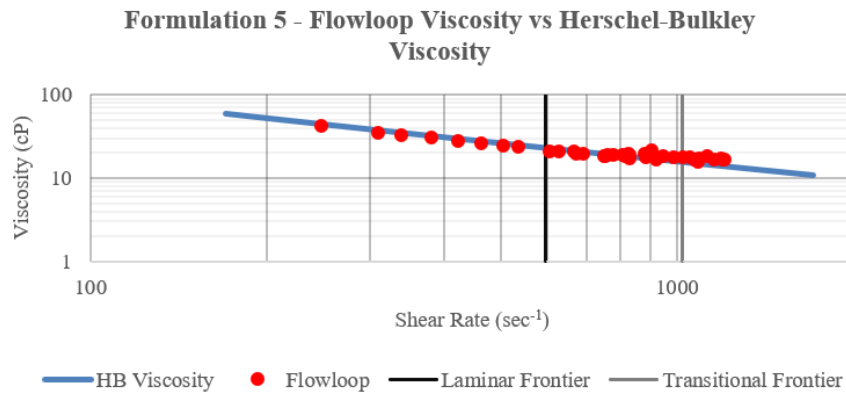

Figure 15: Formulation 5 - Flowloop Viscosity vs Herschel-Bulkley Viscosity

thus, when plotting the boundaries of laminar and turbulent flow regimes, a trend becomes evident. This hypothesis is illustrated in Figures 11-15 presented below.

The difference shown in Figure 11 and Figure 15 is obvious. The Rabinowitsch-Mooney Equation in Appendix A1 is not applicable to turbulent flow regime since Equation (10), used to determine the shear stress at the pipe wall τ_w, was developed for the geometry corresponding to a fully developed laminar flow. This explains why the mismatch is more severe in thinner fluids that develop turbulent flow at lower shear rates. Therefore, it is clear that an additional approach (like proposed Algorithm 2) is required to determine an adequate friction factor for turbulent flow, which would be subsequently used to calculate the fluid viscosity.

For the laminar and transitional regions, Algorithm 1 provides good estimation of fluids' viscosity, which matches the calculation based on the Herschel-Bulkley model very well. However, when the flow becomes turbulent, the viscosity estimation using Algorithm 1 is not accurate, especially for thinner fluids (Formulations 1-3). With the use of Algorithm 2, the inclusion of the Thomas's correlation improved the modelling of fluid viscosity in the turbulent flow region. Nevertheless, there are still some discrepancies between measured one from the viscometer and calculated one using Algorithm 2, which possibly due to some uncertainties, for instance, the friction factor models' accuracy, numerical errors, measurement errors and data quality issues. A wary Fluids Engineer would argue that the rheological readings of Formulation 5 are more in accordance to the rheological profile of a typical drilling mud. Thus, it could be possible to validate the applicability of the estimation of fluid viscosity using the instrumented standpipe concept, by carrying out a statistical analysis of the geometry of the pipes in the surface connections of different drilling rigs, compared to the typical pumping rates used for drilling, in order to define whether the fluid is in most cases in laminar or transitional flow regimes when it travels through the standpipe.

7 Conclusions and future work

With respect to the estimation of Xanthan gum fluid properties, we have experimentally verified the applicability of the Rabinowitsch-Mooney equation for the laminar and transitional regions. Therefore, the major significance of this work is to use simple instrumented setup in measuring fluid pressure losses to estimate the viscosity, especially for transitional and laminar flows. The system proved very effective in monitoring pressure and properties changes in real time. In addition, the setup allows us to evaluate friction factor models for pressure loss calculations. Such setup is also linked to automated drilling with realtime monitoring the fluid properties and adjusting them properly. We have to admit the limitations of our work. The fluids we used are Xanthan gum fluids that have a molecular weight, do not represent real drilling fluids. Water based drilling fluids and oil based drilling fluids will be planned to test in the future. A future continuity of this work is to devise a way to combine both the equations for laminar and transitional flow regimes, and the Thomas's correlation for turbulent flow.

References

[1] Dakhil H and Wierschem A. Measurement low viscosities and high shear rates with a rotational rheometer in a thin-gap parallel-disk configuration. *Applied Rheology*, 24(6):1–6, 2014. doi: 10.3933/applrheol-24-63795.

[2] Duffy JJ, Hill AJ, and Murphy SH. Simple method for determining stress and strain constants for non-standard measuring systems on a rotational rheometer. *Applied Rheology*, 25(4):1–6, 2015. doi: 10.3933/applrheol-25-42670.

[3] Marchesini FH, Naccache MF, Abdu A, Alicke AA, and Mendes P RS. Rheological characterization of yield-stress materials: Flow pattern and apparent wall slip. *Applied Rheology*, 25(5):1–10, 2015. doi: 10.3933/applrheol-25-53883.

[4] Takeh A and Shanbhag S. A computer program to extract the continuous and discrete relaxation spectra from dynamic viscoelastic measurements. *Applied Rheology*, 23(2):1–10, 2012. doi: 10.3933/applrheol-23-24628.

[5] Borg T and Paakkonen EJ. Linear viscoelastic model for different flows based on control theory. *Applied Rheology*, 24(6):1–6, 2015. doi: 10.3933/applrheol-25-64304.

[6] Saasen A and Hodne H. Influence of vibrations on the rheological properties of drilling fluids and its consequence on solids control. *Applied Rheology*, 26(2):1–6, 2016. doi: 10.3933/applrheol-26-25349.

[7] Hernandez JC, Ramirez AG, Duran JDG, Caballero FG, Zubarev AY, and Lopez MTL. On the effect of wall slip on the determination of the yield stress of magnetorheological fluids. *Applied Rheology*, 27(1):1–8, 2016. doi: 10.3933/applrheol-27-15001.

[8] Carmona JA, Calero N, Ramirez P, and Munoz J. Rheology and structural recovery kinetics of an advanced performance xanthan gum with industrial application. *Applied Rheology*, 27(2):1–9, 2017. doi: 10.3933/applrheol-27-25555.

[9] Saasen A and Ytrehus JD. Rheological properties of drilling fluids: Use of dimensionless shear rate in herschel-bulkley and power-law models. *Applied Rheology*, 28(5):1–6, 2018. doi: 10.3933/applrheol-28-54515.

[10] Skadsem HJ and Saasen A. Concentric cylinder viscometer flows of herschel-bulkley fluids. *Applied Rheology*, 29(1):173–181, 2019. doi: 10.1515/arh-2019-0015.

[11] Saasen A, Omland TH, Ekrene SJ, and Breviere J et al. Automated measurement of drilling fluid and drill-cutting properties. *IADC/SPE Drilling Conference*, 2009. doi: 10.2118/112687-PA.

[12] Vajargah AK, Sullivan G, and Van Oort E. Automated fluid rheology and ecd management. *SPE Deepwater Drilling and Completions Conference, Galveston, Texas, USA*, 2016. doi: 10.2118/180331-MS.

[13] Skadsem HJ, Leulseged A, and Cayeux E. Measurement of drilling fluid rheology and modeling of thixotropic behavior. *Applied Rheology*, 29(1):1–11, 2019. doi: 10.1515/arh-2019-0001.

[14] Stock T, Ronaes E, Fossdal T, and Bjerkaas J. The development and successful application of an automated real-time drilling fluids measurement system. *SPE Intelligent Energy International held in Netherlands*, 2012. doi: 10.2118/150439-MS.

[15] Carisen L, Rolland NL, Nygaard G, and Time RW. Simultaneous continuous monitoring of the drilling fluid friction factor and density. *SPE Drilling and Completion*, 28:34–44, 2013. doi: 10.2118/84175-PA.

[16] Cimpan E and Nygaard G. Design and simulation of a small-scale experimental facility for drilling operations. *SIMS*, 2013.

[17] Sui D, Sukhoboka O, and Aadnoy BS. Improvement of wired drill pipe data quality via data validation and reconciliation. *International Journal of Automation and Computing*, 15:625-636, 2017. doi: 10.1007/s11633-017-1068-9.

[18] Madlener K, Frey B, and Ciezki HK. Generalized reynolds number for non-newtonian fluids. *EDP Sciences*, 2009. doi: 10.1051/eucass/200901237.

[19] Nguyen QH and Nguyen ND. Incompressible non-newtonian fluid flows, continuum mechanics - progress in fundamentals and engineering applications. *InTech*, pages 47–72, 2012. doi: 10.5772/26091.

[20] Trinh KT. The instantaneous wall viscosity in pipe flow of power law fluids: Case study for a theory of turbulence in time-independent non-newtonian fluids. *Institute of Food Nutrition and Human Health Massey University, New Zealand*, 2009.

[21] Khalifa HE Kestin J and Correia RJ. Tables of the dynamic and kinematic viscosity of aqueous nacl solutions in the temperature range 20-150°C and the pressure range 0.1-35 mpa. *Journal of Physical and Chemical Reference Data 10, 71. Division of Engineering, Brown University*, 10(1):71–88, 1981. doi: 10.1063/1.555641.

[22] Press WH, Teukolsky SA, Vetterling WT, and Flannery BP. The shooting method in the art of scientific computing. *New York: Cambridge University Press*, 2007.

[23] Metzner AB and Reed J. Flow of non-newtonian fluids – correlation of the laminar, transition and turbulent-flow regions. *AIChE Journal*, 1(4):434–440, 1955. doi: 10.1002/aic.690010409.

Appendix A1

The Rabinowitsch-Mooney Equation permits to calculate viscosity of a Non-Newtonian Herschel-Bulkley fluid in laminar flow by converting flow rate to shear rate. The flow rate through the pipe can be shown as

$$Q = \int_0^R 2\pi r v(r) dr \qquad (A1)$$

where Q is flow rate, R is pipe radius and v is velocity. It becomes

$$Q = v(r)\pi r^2 |_0^R - \int_0^R \pi r^2 \left(\frac{dv}{dr}\right) dr.$$

Since no slip at the wall, so $v = 0$ when $r = R$, the first term of the above equation is zero. We have

$$Q = - \int_0^R \pi r^2 \left(\frac{dv}{dr}\right) dr.$$

Since

$$\gamma = -\frac{dv}{dr}, dr = \frac{R}{\tau_w} d\tau.$$

The above two relationships are inserted into $Q = -\int_0^R \pi r^2 (\frac{dv}{dr}) dr$. It becomes

$$Q = \frac{\pi R^3}{\tau_w^3} \int_0^{\tau_w} \tau^2 \gamma d\tau. \qquad (A2)$$

For flow in a pipe, the shear rate γ is negative so the integral in Equation (A2) becomes positive. For a given relationship between shear stress τ and shear rate γ, the value of the integral depends only on the value of shear stress in the pipe wall τ_w. The flow rate, Q can be expressed as

$$Q = \pi R^2 v. \qquad (A3)$$

Combine it with the equation (A2), we have

$$\frac{8v}{D} = \frac{4}{\tau_w^3} \int_0^{\tau_w} \tau^2 \gamma d\tau. \qquad (A4)$$

It is convenient first to multiply Equation (A4) by τ_w^3 throughout,

$$\frac{8v}{D} = 4 \int_0^{\tau_w} \tau^2 \gamma d\tau. \qquad (A5)$$

Then differentiating with respect to τ_w to obtain [19]:

$$3\tau_w^2(\frac{8v}{D}) + \tau_w^3 \frac{\partial(\frac{8v}{D})}{\partial \tau_w} = 4\tau_w^2 \gamma_w. \qquad (A6)$$

Solving Equation (A6) with respect to the wall shear rate γ_w,

$$\gamma_w = (\frac{8v}{D})[\frac{3}{4} + \frac{1}{4}\frac{\tau_w}{(\frac{8v}{D})}\frac{\partial(\frac{8v}{D})}{\partial \tau_w}] \qquad (A7)$$

Now, based on the relation given below

$$\frac{\partial(\ln x)}{\partial x} = \frac{1}{x} \rightarrow \partial(\ln x) = \frac{\partial x}{x}. \qquad (A8)$$

Combining Equations (A7) and (A8), the Rabinowitsch-Mooney Equation is given as follows:

$$\gamma_w = \frac{8v}{D}[\frac{3}{4} + \frac{1}{4}\frac{\partial\ln(\frac{8v}{D})}{\partial(\ln \tau_w)}] \qquad (A9)$$

It can be reformulated as:

$$\gamma_w = \frac{8v}{D}\frac{3n_a + 1}{4n_a} \qquad (A10)$$

where n_a is a generalized flow index given by:

$$n_a = \frac{\partial(\ln \tau_w)}{\partial \ln(\frac{8v}{D})}. \qquad (A11)$$

Appendix A2

The model presented by Metzner and Reed [23] by formulating a generalized Reynolds number valids for Herschel-Bulkley fluids. The equations are given as follows [23]:

$$Re_g = \frac{\rho v D_{eff}}{\mu_a}, \qquad (A12)$$

where D_{eff} is the effective inner diameter of the pipe, which is given as

$$D_{eff} = \frac{4n_a}{3n_a + 1}D. \qquad (A13)$$

The generalized flow index is given by

$$n_a = \frac{nK(\frac{8v}{D})^n}{\tau_0 + nK(\frac{8v}{D})^n}, \qquad (A14)$$

where τ_0 is yield point, K is consistency coefficient, n is the flow index. The apparent viscosity can be expressed by

$$\mu_a = \tau_0(\frac{8v}{D_{eff}})^{-1} + K(\frac{8v}{D_{eff}})^{n-1}. \qquad (A15)$$

Once the appropriate expression to determine the Reynolds number for Herschel-Bulkley fluids has been defined, we can finally describe the flow regime in the pipe based on the guidelines given for Newtonian fluids. For laminar flow

$$f = \frac{64}{Re_g}. \qquad (A16)$$

Table A1: Friction factor correlations for Non-Newtonian fluids in turbulent flow [20]

Author	Year	Models
Dodge and Metzner	1959	$1/\sqrt{f} = \frac{4}{n_a^{0.75}} \log(Re_g f^{1-n_a/2}) - \frac{0.4}{n_a^{1.2}}$
Shaver and Merill	1959	$f = \frac{0.079}{n_a^5 Re_g^{\frac{2.63}{10.5^{n_a}}}}$
Thomas	1960	$1/\sqrt{f} = \frac{4}{n_a} \log(Re_g f^{1-n_a/2}) - 0.4 n_a$
Clapp	1961	$1/\sqrt{f} = \frac{4.53}{n_a} \log(Re_g f^{1-n_a/2}) - \frac{2.69}{n_a} + 0.68(5n_a - \frac{8}{n_a})$
Trinh	1969	$1/\sqrt{f} = \frac{4.06}{n_a} \log(Re_g f^{1-n_a/2}) - \frac{2.78}{n_a} + 2.16$
Hanks and Ricks	1973	$f = \frac{0.0682 n_a^{-0.5}}{Re_g^{\frac{1}{1.87+2.39n_a}}}$
Shenoy and Saini	1986	$1/\sqrt{f} = 3.57 \log(\frac{Re_g^{n_a^{-0.615}}}{6.5^{-(1+0.75n_a)}})$
El-Eman et al	2003	$f = \frac{1}{4} \frac{n_a}{(3.072 - 0.1433 n_a) Re_g^{n_a/(0.282-4.211n_a)} - 0.00065}$

For turbulent flow, friction factor model is required to determine an adequate friction factor, which would be subsequently used to calculate the fluid viscosity. Several models available in the literature were analysed, they are presented in Table A1 [20] shown below. The concept of frictional pressure losses derives from the resistance experienced by fluids flowing through pipes caused by friction against the pipe wall. The frictional pressure loss is determined from the Darcy-Weisbach equation given below.

$$\Delta P_{\text{Frictional}} = \frac{fL\rho v^2}{2D}. \tag{A17}$$